Journal of Biomedical Optics

SPIEDigitalLibrary.org/jbo

Spatiotemporal and time-frequency analysis of functional near infrared spectroscopy brain signals using independent component analysis

Zhen Yuan

SPIE

Spatiotemporal and time-frequency analysis of functional near infrared spectroscopy brain signals using independent component analysis

Zhen Yuan
University of Macau, Bioimaging Core, Faculty of Health Sciences, Av. Padre Tomás Pereira, Taipa, Macau SAR, China

Abstract. Functional near infrared spectroscopy (fNIRS) is a noninvasive method to capture brain activities according to the measurements of changes in both oxyhemoglobin and deoxyhemoglobin concentrations. However, fNIRS recordings are the hemodynamic signals that come from the latent neural sources that are spatially and temporally mixed across the brain. The purpose of this work is to extract the temporal and frequency characteristics as well as the spatial activation patterns in the brains using independent component analysis (ICA). In this study, the filtered fNIRS recordings were processed and the time-frequency and spatiotemporal domain independent components (ICs) were identified by ICA. We found that multiple task-related components can be separated by ICA in time-frequency domain, and distinct spatial patterns of brain activity can be derived from ICs that are well correlated with the specific neural events, such as finger tapping tasks.
[DOI: 10.1117/1.JBO.18.10.106011]

Keywords: independent component analysis; functional near infrared spectroscopy; neuroimaging; signal processing methods; cognitive neurosciences.

Paper 130439R received Jun. 26, 2013; revised manuscript received Aug. 28, 2013; accepted for publication Sep. 20, 2013; published online Oct. 22, 2013.

1 Introduction

Since the mid-1970s, functional near infrared spectroscopy (fNIRS) has been developing a noninvasive technique to investigate brain activities under different stimuli by measuring the absorption coefficients of the near-infrared light between 650 and 950 nm.[1–9] Compared to other functional imaging modalities, such as functional magnetic resonance imaging (fMRI) and positron emission tomography (PET), fNIRS is able to offer unsurpassed high temporal resolution and provide quantitative information for both oxyhemoglobin and deoxyhemoglobin, which is essential for revealing the rapid changes of dynamic patterns in the brain including changes of blood oxygen, blood volume, and blood flow.

Recently, independent component analysis (ICA) has been recognized as a tool for evaluating the hidden spatiotemporal sources from electroencephalography (EEG) and fMRI measurements. ICA also shows its potential for analyzing the time-frequency domain independent components (ICs) of fNIRS recordings.[10–16] However, the previous work based on the time-frequency ICA is mainly confined to remove the physiological noise or artifacts from the raw fNIRS signals. The separation of brain activation patterns in time-frequency domain is generally not addressed, which presents one of the main challenges for understanding brain dynamics based on fNIRS measurements. In addition, the spatiotemporal ICA has been proposed for extracting the ICs from fNIRS signals.[13,17] However, questions about identifying the most important components and separating regions of interests (ROIs) from brain networks are not resolved by most of the developed methods. Further, the event-related spectral amplitude, phase and coherence perturbation based on ICA are not assessed by most of the available fNIRS techniques, which makes it very difficult for us to extract the ICs accounting for the largest portions of brain oscillations and brain synchronization in frequency domain.

In this study, we will further the popular ICA tool in fNIRS to simultaneously analyze the spatiotemporal and time-frequency domain ICs. In particular, we will combine run-by-run visualization in time-frequency domain and two-dimensional (2-D) brain map visualization in space to show the extracted unmixed components of brain activity. The developed fNIRS data analysis methods based on ICA will provide us a robust tool to capture the complex brain dynamics and brain oscillations in spatiotemporal and time-frequency domains.

2 Materials and Methods

2.1 *Theory Model for fNIRS*

According to Beer's law,[1] the wavelength-dependent tissue optical density changes can be written in terms of the concentration changes of the chromophores including HbO_2 and HbR at time t and wavelength λ,

$$\begin{bmatrix} \Delta \mathrm{OD}(r,t)|_{\lambda_1} \\ \Delta \mathrm{OD}(r,t)|_{\lambda_2} \end{bmatrix} = \mathrm{DPF}(r) l(r) \begin{bmatrix} \varepsilon_1(\lambda_1) & \varepsilon_2(\lambda_1) \\ \varepsilon_1(\lambda_2) & \varepsilon_2(\lambda_2) \end{bmatrix} \begin{bmatrix} \Delta \mathrm{HbO}_2(r,t) \\ \Delta \mathrm{HbR}(r,t) \end{bmatrix} \quad (1)$$

in which ΔOD is the optical density change (unitless quantity) at the position r, $\mathrm{DPF}(r)$ is the unitless differential path length factor, $l(r)$ (mm) is the distance between the source and the detector, $\varepsilon_i(\lambda)$ is the extinction coefficient of the i'th chromophore at wavelength λ of laser sources, and ΔHbO_2 and ΔHbR (μM) are

Address all correspondence to: Zhen Yuan, University of Macau, Faculty of Health Sciences, Av. Padre Tomás Pereira, Taipa, Macau SAR, China. Tel: 85383978445; Fax: 85383978500; E-mail: zhenyuan@umac.mo

0091-3286/2013/$25.00 © 2013 SPIE

the chromophore concentration change for oxy- and deoxyhemoglobin, respectively. After multiplying the inverse matrix of the extinction coefficients for both sides of Eq. (1), the time series matrix for the changes of HbO_2 and HbR is written as

$$\begin{bmatrix} \Delta\mathrm{HbO}_2(r,t) \\ \Delta\mathrm{HbR}(r,t) \end{bmatrix} = \begin{bmatrix} Q_{\mathrm{HbO}_2}(r,t) \\ Q_{\mathrm{HbR}}(r,t) \end{bmatrix} / [\mathrm{DPF}(r) l(r)] \quad (2)$$

in which $\boldsymbol{Q}(r,t)$ vectors are the product of the inversion matrix of the extinction coefficient and the optical density change vectors. Based on these, the change of total hemoglobin concentration ΔHbT (μM) is defined as the sum of ΔHbO_2 and ΔHbR.

2.2 *Independent Component Analysis*

The ICA algorithm employed in this study is infomax ICA algorithm,[18] which separates mixed signals into maximally independent sources by maximization of information transfer between them.[19]

2.2.1 *Theoretical framework for spatiotemporal ICA*

Since fNIRS recordings are from K channels with M dimensional random time vector for each channel, the measurement matrix for $\boldsymbol{\Delta HbO_2}(r,t)$ is denoted by

$$\boldsymbol{\Delta HbO_2} = \begin{bmatrix} \Delta\mathrm{HbO}_2(r_1,t_1) & \Delta\mathrm{HbO}_2(r_1,t_2) & \dots & \Delta\mathrm{HbO}_2(r_1,t_M) \\ \Delta\mathrm{HbO}_2(r_2,t_1) & \Delta\mathrm{HbO}_2(r_2,t_2) & \dots & \Delta\mathrm{HbO}_2(r_2,t_M) \\ \vdots & \vdots & \vdots & \vdots \\ \Delta\mathrm{HbO}_2(r_K,t_1) & \Delta\mathrm{HbO}_2(r_K,t_2) & \dots & \Delta\mathrm{HbO}_2(r_K,t_M) \end{bmatrix}. \quad (3)$$

$\boldsymbol{\Delta HbO_2}$ is then decomposed by ICA, estimating the optimal inverse of the mixing matrix $\boldsymbol{A}$ and a set of source time courses $\boldsymbol{S}$. In terms of ICA estimation, $\boldsymbol{\Delta HbO_2}$ is further written as[18]

$$\boldsymbol{\Delta HbO_2} = \boldsymbol{AS} \quad (4)$$

in which $\boldsymbol{A}$ is the K-by-N mixing matrix, N is the number of unmixed sources and $\boldsymbol{S}$ is the N-by-M time courses of different ICs. Typically, we utilize $K \geq N$ so that A is of full rank. The goal of ICA is to estimate an unmixing matrix $\boldsymbol{W}_{N\times K}$ such that $\boldsymbol{X}$ is given by

$$\boldsymbol{X} = \boldsymbol{W}[\boldsymbol{\Delta HbO_2}(r)] \quad (5)$$

in which $\boldsymbol{X}$ is a good approximation of the "true" neural sources $\boldsymbol{S}$ and the inversion of weighted matrix $\boldsymbol{W}$ will extract the brain activity maps of the unmixed spatial sources. The unmixing matrix $\boldsymbol{W}$ (i.e., the inversion of $\boldsymbol{A}$) is the most important matrix in ICA and the infomax ICA algorithm uses the gradient ascent iteration algorithm to compute $\boldsymbol{W}$ by maximizing the entropy of the output of a single-layer neural network. The resulting updated equation for the algorithm to calculate $\boldsymbol{W}$ is

Step 1: $\boldsymbol{W}(0)$ (e.g., random)
Step 2: $\boldsymbol{W}(t+1) = \boldsymbol{W}(t) + \eta(t)[\boldsymbol{I} - \boldsymbol{y}(\boldsymbol{X})\boldsymbol{X}^T]\boldsymbol{W}(t)$
Step 3: If not converged, go back to step 2

in which t represents a given approximation step, $\eta(t)$ is a general function that specifies the sizes of the steps for the unmixing matrix updates (usually an exponential function or a constant), I is the identity matrix, T is the transposition operator, and $\boldsymbol{y}(\boldsymbol{X}) = g(\boldsymbol{X})$ and $g(x) = 1/(1+\mathrm{e}^{-x})$ is the nonlinearity in the neural network if the right type of distribution $\boldsymbol{X}$ is not clear. However, in the case of super-Gaussian distribution, $\boldsymbol{y}(\boldsymbol{X})$ is usually set to $\boldsymbol{y}(\boldsymbol{X}) = \tan h(\boldsymbol{X})$; and for the sub-Gaussian distribution, $\boldsymbol{y}(\boldsymbol{X})$ is usually set to $\boldsymbol{y}(\boldsymbol{X}) = \boldsymbol{X} - \tan h(\boldsymbol{X})$.[20] After spatiotemporal ICA, we will get the time course and spatial activation patterns of each IC identified from ΔHbO_2 measurements. Likewise, we can extend the ICA method to analyze the independent sources for the change of HbR and HbT.

2.2.2 *Theoretical framework for time-frequency ICA*

Extensive investigations in EEG have validated that stimuli induce not only time-locked responses but also phase- and frequency-related brain oscillatory activities quantified by power spectrum, event-related spectral perturbation (ERSP) and intertrial coherence (ITC) for different ICs or channels.[19] To assess event-related spectral amplitude, phase and coherence perturbations for the time courses of ICs identified from fNIRS recordings, we will measure the baseline, epoch-mean power spectrum, and two event-related time–frequency parameters: (1) ERSP, which represents the mean event-related changes in the power spectrum for a specific IC; (2) ITC, which is a frequency-domain measure of the partial or exact synchronization of activity at a particular latency and frequency to a set of experimental events to which fNIRS data runs are time locked for different ICs. To determine the oscillatory activity with fNIRS recordings, the complex exponential form of the sinusoidal wavelet [short time discrete Fourier transform (ST-DFT)] was used to analyze the power spectrum and the phase spectral properties. So in terms of ST-DFT, the time-frequency analysis for the spectral estimation $F(f,t)$ from the measurements x with window function Win[19] is written as

$$F(f,t) = \int x(u)\mathrm{Win}(u-t)\exp[-j2\pi f(u-t)]\mathrm{d}u \quad (6)$$

in which the measurement x is the element of the time course vector for a single IC obtained from Eq. (5), t is time and f is the frequency. The window function Win is commonly a Hann window or a Gaussian window bell centered around zero and detailed description about this operation can be found in MATLAB package, $F(f,t)$ is calculated over a sliding time window with variable u, the power spectrum is defined as the square of $F(f,t)$, and we generally adopt the log deviations from epoch-mean power at a specific frequency as our displayed power spectrum.[19]

Quantification of the ERSP requires calculating the power spectrum over a sliding time window and then averaging across data runs. Typically, for n-run measurements, if $F_k(f,t)$ is the spectral estimation of run k at frequency f and time t, ERSP is written as

$$\mathrm{ERSP}(f,t) = \frac{1}{n}\sum_{k=1}^{n} |F_k(f,t)|^2. \quad (7)$$

It is noted that to visualize power changes across the frequency range, we will subtract the mean baseline log power spectrum from each spectral estimate, producing the baseline-normalized ERSP.[19]

ITC is defined as

$$\mathrm{ITC}(f,t) = \frac{1}{n}\left|\sum_{k=1}^{n} \frac{F_k(f,t)}{|F_k(f,t)|}\right|. \quad (8)$$

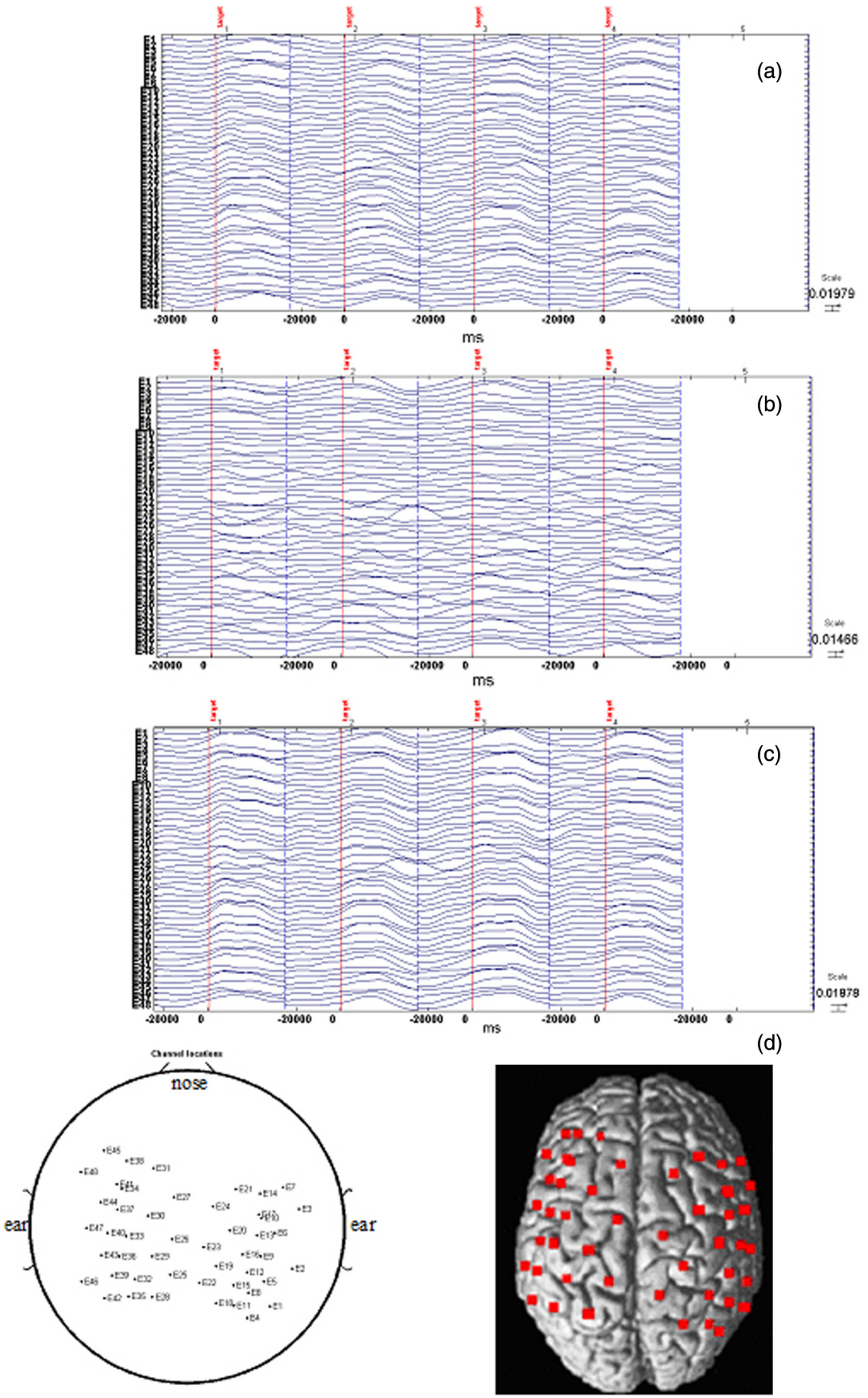

Fig. 1 The data reviews for filtered HbO_2 measurements (a), HbR measurements (b) and HbT measurements (c). Channel configurations in two-dimension (2-D) (left column) and three-dimension (3-D) (right column) (d). Here, four-run fNIRS recordings (separated by dashed lines) are plotted at 48 channel sites (channel names on the left) and the onset time for right finger tapping is marked as "target."

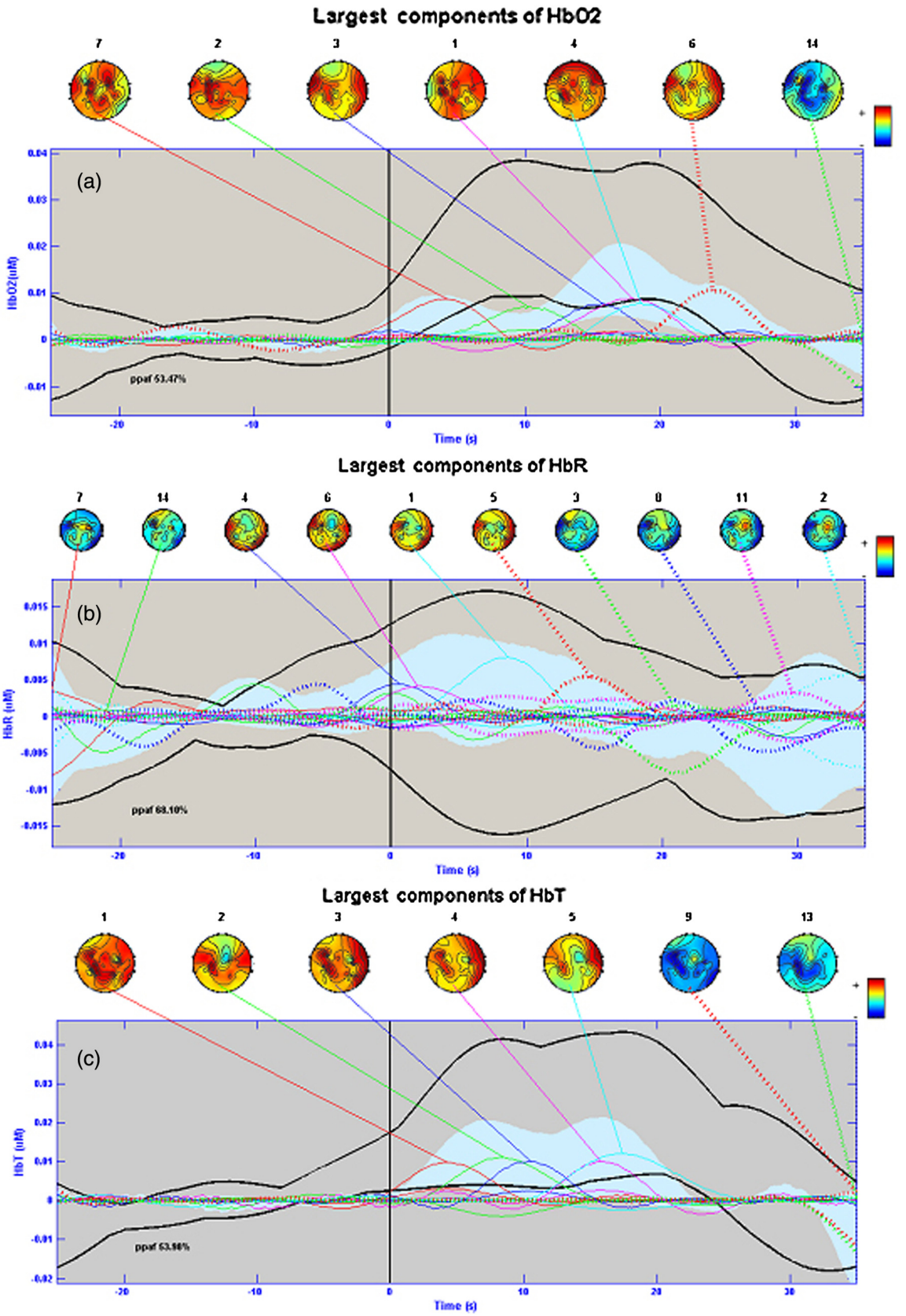

Fig. 2 The spatiotemporal analysis of independent components (ICs) that contribute the most to the HbO_2 measurements (a), HbR measurements (b), and HbT measurements (c). Brain activity maps in 2-D are also provided and the cortical activity was mostly seen in the left primary motor cortex and supplementary motor area (SMA) (see detailed images in Fig. 3). The black thick lines indicate the data envelope (i.e., minimum and maximum of all channels at every time point) and the colored lines show the components of different chromophores.

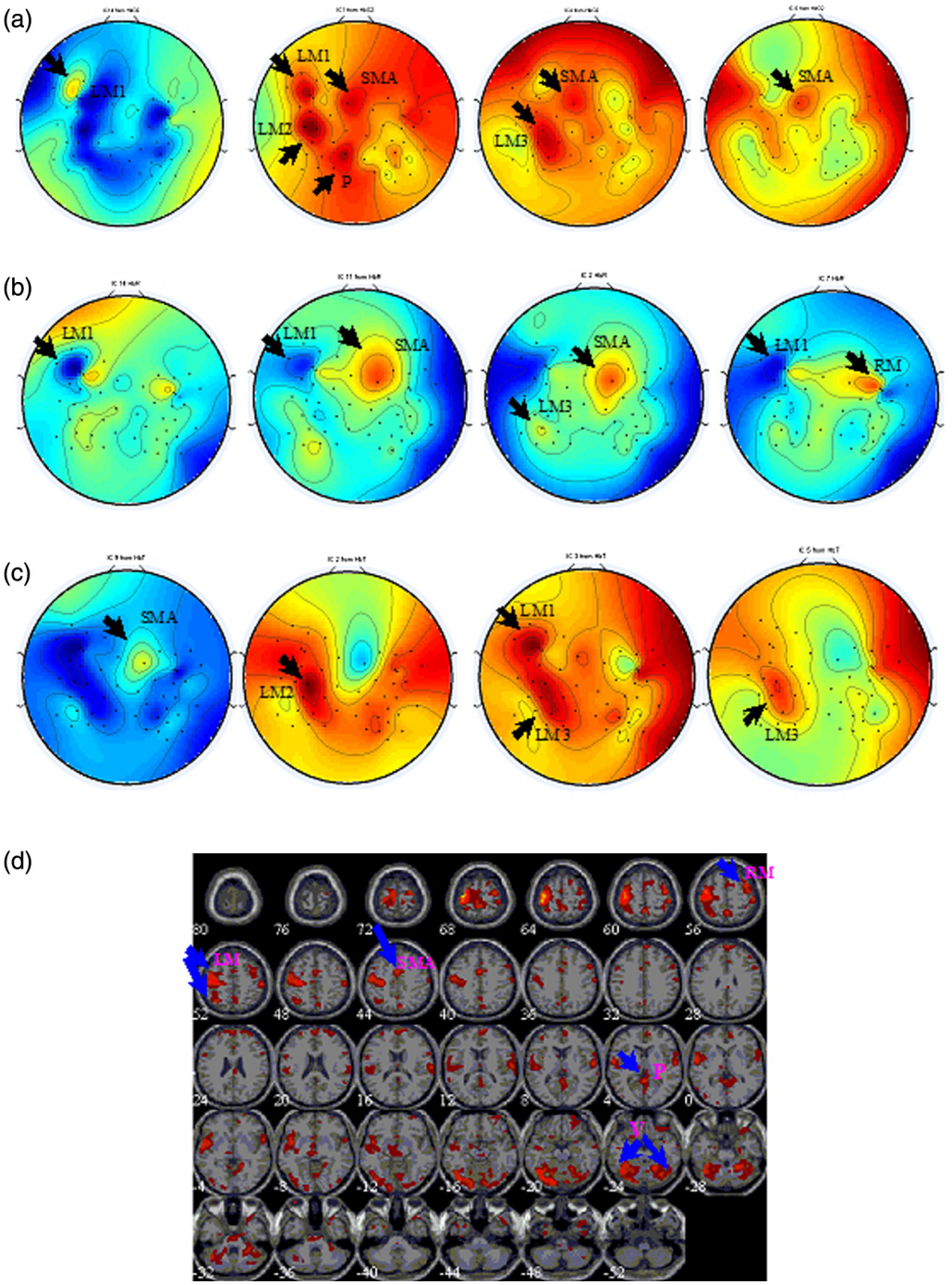

Fig. 3 The most significant ICs calculated from HbO_2 measurements (a), HbR measurements (b), and HbT measurements (c). The composite ICs for each specific chromophore will generate its ROIs for right finger tapping tasks. (d) The fMRI image for one subject who performed right finger tapping tasks. The cortical activity was mostly seen in the left primary motor cortex and SMA and the fNIRS findings correlated well with the fMRI features. LM: left primary motor cortex; LM1: left primary motor cortex 1; LM2: left primary motor cortex 2; LM3: left primary motor cortex 3; SMA: supplementary motor area; RM: right primary motor cortex; P: parietal cortex; and V: visual cortex.

2.3 *Experimental Systems and Data Acquisition*

The fNIRS tests are implemented with a block design for a right finger tapping task. The experiment is performed using a 48-channel FOIRE-3000 (Shimadzu OMM) system, which has 16 sources, 16 detectors, and 48 channels. In this system, two continuous wave lights at wavelengths 780 and 856 nm are emitted at each source fiber. In the case of block design for right finger tapping tasks, the onset time for the first trigger was at 20 s and then followed by a 20-s period of activation alternated with a 40-s period of rest. This was repeated four times for the subject. The onset time for the last trigger was at 260 s and the duration was 20 s, followed by a 20-s period of rest. As such, the total recording time was 300 s. During the task period, the subject was instructed to perform a finger flexion and extension action repeatedly. Data segmentation, which is also known as epoching in signal processing, is utilized to

chop up the continuous fNIRS data into small time periods. The general way to do this is to extract segments surrounding the event codes from the experiments, e.g., from −25 s prior to the event onset until 35 s after the event code in this study. The original photon density datasets could be downloaded freely from http://bisp.kaist.ac.kr/NIRS-SPM/Sample_data.[20] The converted HbO_2, HbR, and HbT change measurements (DPF = 4, sampling rate = 7.7 Hz) are filtered, segmented, and displayed in Figs. 1(a)–1(c), respectively. The configurations of 48 channels located on the scalp are also provided in Fig. 1(d). It is seen from Fig. 1 that significantly higher increases in ΔHbT and ΔHbO_2 in the motor cortex were observed during the stimulus processing for the finger tapping tasks in comparison with those from rest states. However, this is not the case for ΔHbR, in which we found a significant decrease during the stimulus processing when compared with the measurement from baselines.

3 Results and Discussion

3.1 *Spatiotemporal Analysis of fNIRS Signals Using ICA*

For all the four-run fNIRS recordings (five onsets with period of 300 s) of right finger tapping tasks, the 2-D brain activity maps and associated IC time courses were first identified by ICA from the filtered HbO_2, HbR and HbT change measurements. To quantify the contribution of ICs to HbO_2, we plot in Fig. 2(a) the components that contribute the most to it in terms of the most HbO_2 variance of all the 48 ICs, where we observed ICs 1–4, 6, 7, and 14 are the most significant ones. However, we found that only ICs 1, 4, 6, and 14 correlate well with right finger tapping tasks since ICs 2, 3, and 7 basically identify noise or unrelated neural events. The brain activity maps of ICs 1, 4, 6, and 14 are the identified ROIs for HbO_2. We also capture the components that contribute the most to the filtered HbR and HbT measurements, which are provided in Figs. 2(b) and 2(c), respectively.

In addition, the ROIs identified by ICA from different chromophores are provided in Fig. 3, where we found that the ROIs for right finger tapping tasks are mainly located in the left primary motor cortex and supplementary motor area. However, we did observe identified brain activities located in the parietal cortex for HbO_2 or in the right motor cortex for HbR. These findings show good agreement with neural physiologies for a right finger tapping task.[3,9] We also reconstructed the brain images for a different subject using fMRI data with the right finger tapping tasks (fMRI datasets can be downloaded from http://bisp.kaist.ac.kr/NIRS-SPM).[21] We found the ROIs of fNIRS correlate very well with fMRI findings while the recordings are acquired from different subjects, which validate that ICA is able to

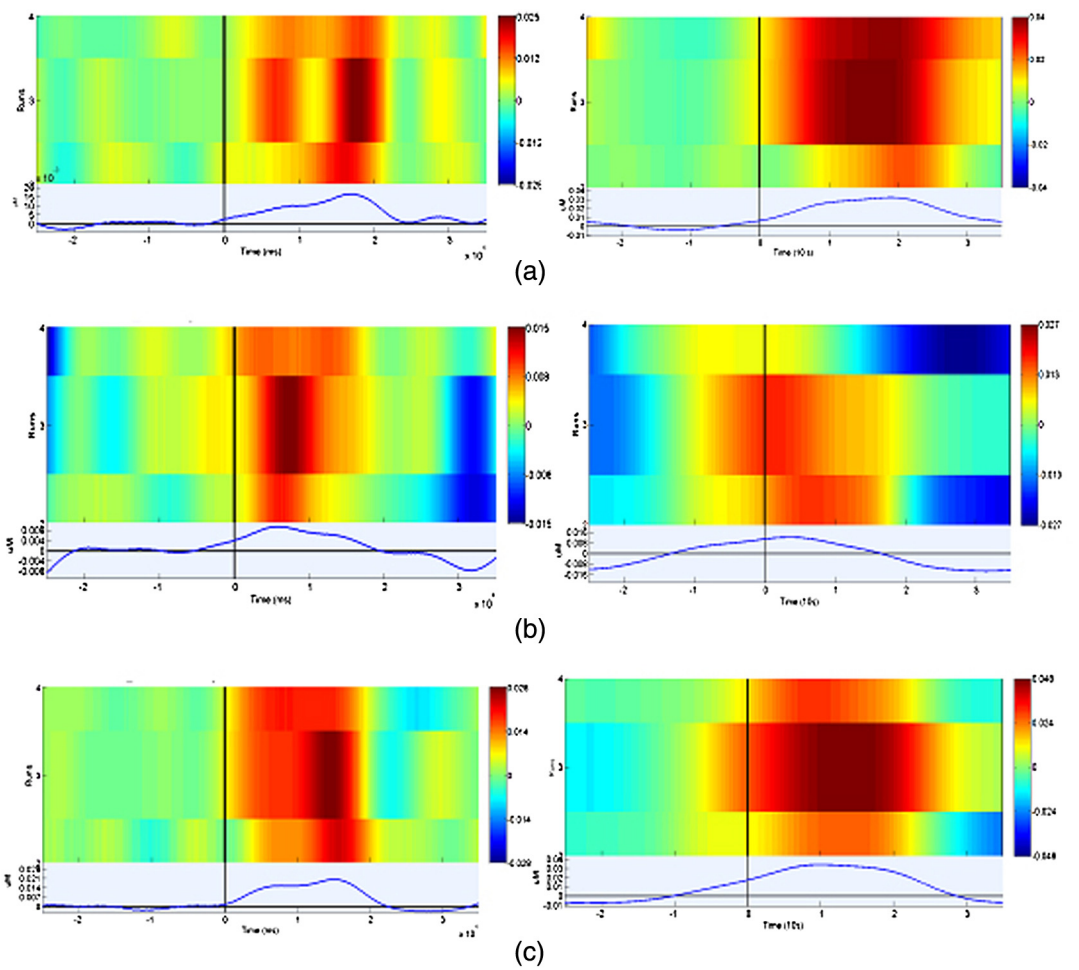

Fig. 4 Run by run visualization in temporal domain for the HbO_2 measurements (a), HbR measurements (b) and HbT measurements (c) processed with ICA (left column of the images) and without ICA (right column of the images). The images on the left column show the correct onset time (0 s) and stimulus duration (0 to 20 s). Runs were imaged in (bottom-to-top) order of their occurrence during the experiment for an arbitrary selected channel 41. The bottom curve of each figure shows the run-averaged time series of fNIRS recordings for each chromophore.

effectively capture the spatial maps of brain activity using fNIRS recordings. Further work that combines the IC time courses and NIRS-SPM[9] is being done to achieve high resolution and 3-D ICs imaging.

To display the hemodynamic response distributions processed by ICA, runs were imaged in (bottom-to-top) order of their occurrence during the experiment. Figure 4 shows their distribution in an arbitrary selected channel 41 after we remove the unrelated ICs including artifacts or physiological noise. The bottom curve of each figure in Fig. 4 shows the run-averaged time series of fNIRS recordings for each chromophore. Compared with the datasets processed without ICA shown on the right column of Fig. 4, the new datasets on the left column show correct run duration (0 to 20 s) and accurate onset time (0 s), which validates that the ICA has the capabilities for extracting the correct components during stimulus processing in temporal domain.

3.2 *Time-Frequency Analysis of fNIRS Signals Using ICA*

It is more interesting to look at time-frequency decompositions of component activations than of separate channel activity since ICs may directly index the activity of one brain fNIRS source, whereas channel activities acquire hemodynamic signals from different areas of the brain. We demonstrate how one can use a time-frequency domain ICA to potentially aid in the understanding of the neuromotor process underlying repetitive finger tapping. In Figs. 5(a)–5(c), we plot the ICs that account for the largest portions of brain oscillations with frequencies at 3.5 and 1.2 Hz for HbO_2, HbR, and HbT, respectively. The ICs in frequency domain are sorted and selected in terms of their percentage contributions of total data power. Our studies have shown that synchronized delta frequency (0 to 3 Hz) oscillations are involved in a simple finger tapping task with fNIRS measurements. In particular, the brain oscillatory activities around 1.7/2.6/3.5 Hz are very significant compared those from other frequency bands. Interestingly, it was observed from the right column of Fig. 5 that the ROIs for right finger tapping tasks around 3.5 Hz are found mainly in the left primary motor cortex. However, this is not the case for the brain activation patterns around 1.2 Hz, in which ROIs are not related with the left motor cortex, as displayed on the left column of Fig. 5. It is observed from Fig. 5 that the most significant brain oscillatory activity was mainly found in the left primary motor cortex, which is well correlated with the right finger tapping tasks.

ERSP is able to capture the mean changes in spectral power at each time during the run and at each frequency. In terms of the ERSP distributions shown in Fig. 6, representative IC4 (the brain activity from the fourth IC is well correlated with right

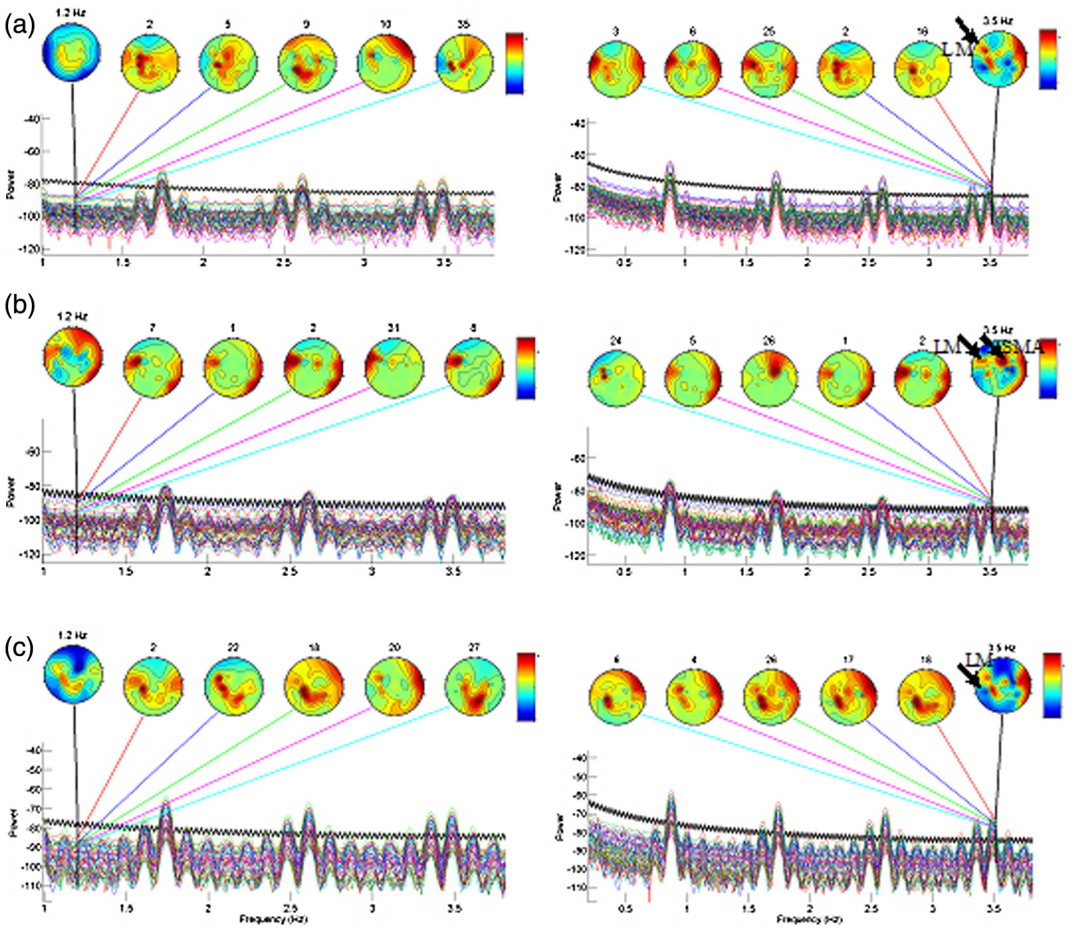

Fig. 5 The ICs accounting for the largest portions of powers of brain oscillatory activities with frequencies at 1.2 Hz (images on the left column) and 3.5 Hz (images on the right column) for HbO_2 measurements (a), HbR measurements (b) and HbT measurements (c). The brain oscillations at 3.5 Hz correlated very well with the right finger tapping tasks for all of the three chromophores. LM: left primary motor cortex and SMA: supplementary motor area.

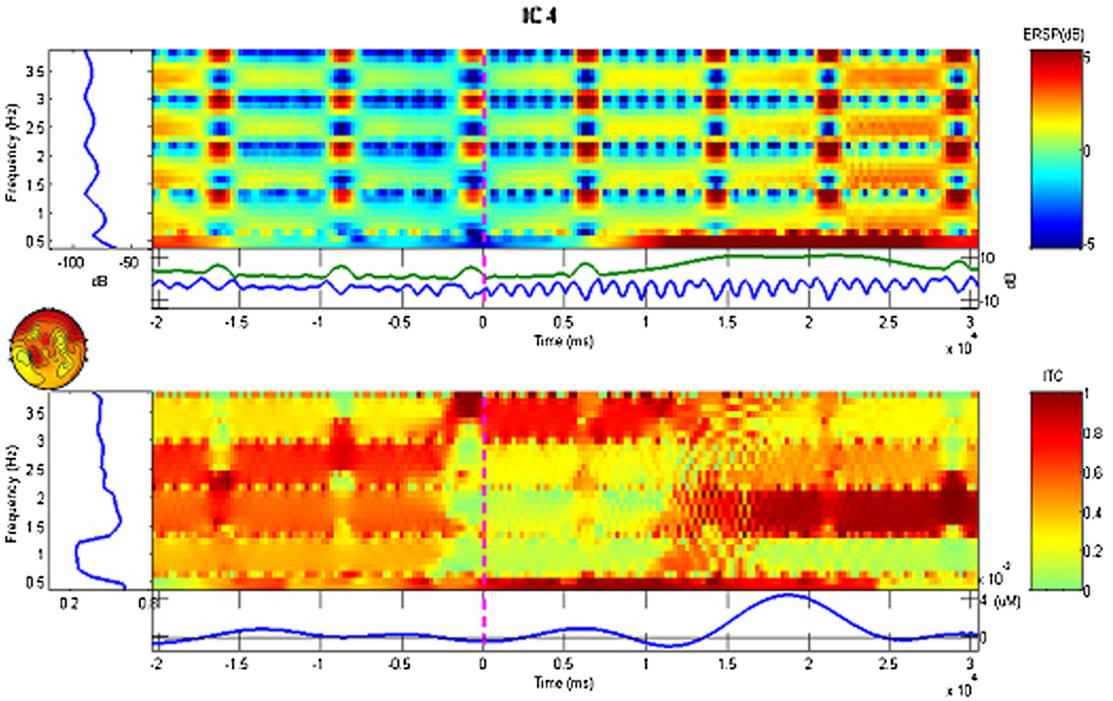

(a) The computed ERSP and ITC for IC4 from HbO_2 Measurements

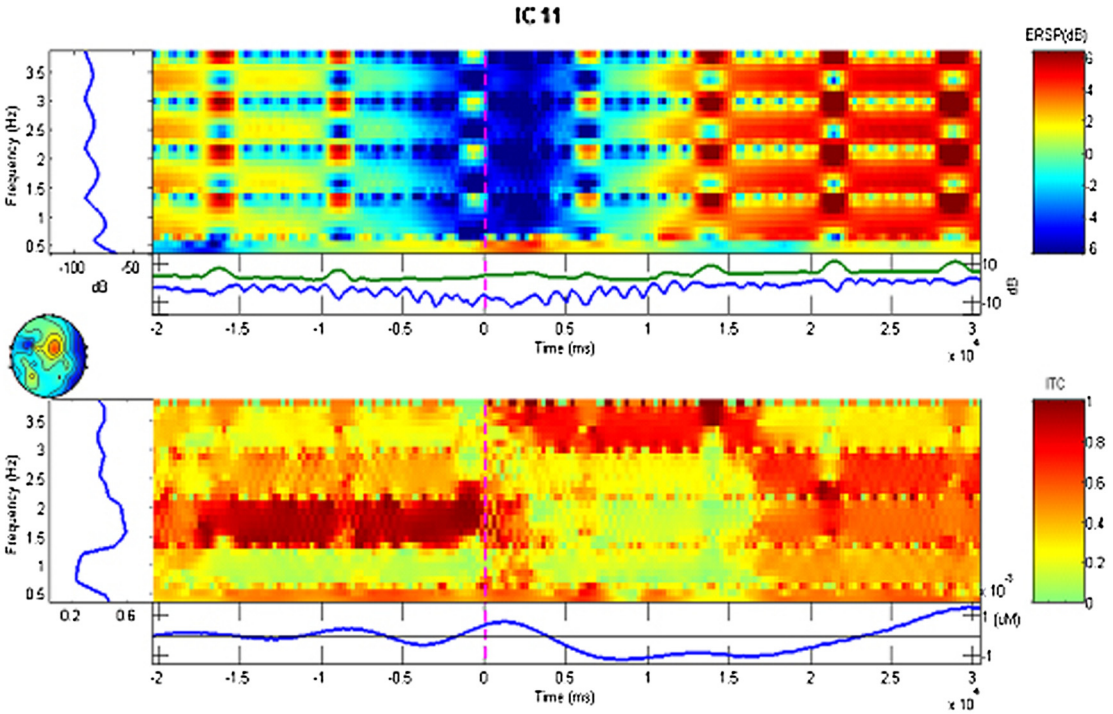

(b) The computed ERSP and ITC for IC11 from HbR Measurements

Fig. 6 Event-related spectral perturbation (ERSP) plots the mean changes in spectral power at each time during the run and at each frequency. The IC4 (the fourth IC) of HbO_2 shows increased ERSP during the stimulus processing with frequencies at 0.7/1.7/2.6/3.5 Hz, whereas IC11 of HbR first shows the decreased ERSP centered at the onset time and then later increased ERSP till the end of the duration with frequencies at 0.7/1.7/2.6/3.5 Hz. The brain activities for IC4 and IC11 become partially synchronized around 3.5 Hz during the stimulus period of 0 to 15 s. However, the brain activities for IC4 become partially synchronized around 1.7 Hz during the stimulus period of 15 to 30 s, whereas IC11 from HbR becomes partially synchronized around 1.7 Hz before the onset of trigger (−15 to 0 s) and around 1.7/2.6 Hz during the stimulus processing. The left curve in the ERSP panel shows the baseline mean power spectrum, whereas the lower curve of the ERSP panel shows the ERSP envelope [low (in blue) and high (in green) mean decibel values, relative to baseline, at each time in the run]. The left curve in intertrial coherence (ITC) panel shows the distributions of mean ITC at different frequencies, whereas the bottom curve in ITC panel shows the run-averaged time course of IC4 or IC11 in micormolar. (a) The computed ERSP and ICTC for IC4 from HbO_2 measurements and (b) the computed ERSP and ITC for IC11 from HbR measurements.

finger tapping tasks) from HbO_2 shows increased ERSP near delta frequency band (1 to 3 Hz) during the stimulus processing (5 to 30 s), whereas representative IC11 from HbR shows a power decrease in the time range (−5 to 10 s), then followed by an increase during the stimulus processing (10 to 30 s). According to the distributions of ITCs plotted in Fig. 6 the brain activities from both HbO_2 and HbR components appear to become partially synchronized around 3.5 Hz during the stimuli period from 0 to 15 ms after the onset of finger tapping tasks. However, brain activities for IC4 from HbO_2 become partially synchronized around 1.7 Hz during the stimulus period (15 to 30 s) while IC11 from HbR becomes partially synchronized around 1.7 Hz before the onset of trigger (−15 to 0 s) and around 1.7/2.6 Hz during the stimulus processing.

3.3 *Comparisons of Different ICA Methods for fNIRS Signal Analysis*

The MATLAB tool packages have over 20 available ICA algorithms.[22] We calculated and compared the recovered ICs using four popular ICA methods including infomax, jade, sobi, and acsobiro. The calculated results using infomax based on HbT measurements are shown in Fig. 7(a), whereas Figs. 7(b)–7(d) show the most important ICs computed from methods 2 to 4. By estimating the spatiotemporal profiles of ICs, we found the recovered ICs using infomax are in good agreement with those from methods 2 to 4. The brain activity areas identified by methods 1 to 4 were mainly found in the left motor cortex, which correlate well with the neurophysiology mechanism for a right finger tapping task. Consequently, there are no significant differences for the reconstructed ICs from the four methods though minor calculation errors among them do exist. It seems that infomax, jade, and acsobiro capture similar distribution of HbT components compared with that from the sobi method. If we compare the recovered ICs 2 and 5 from jade with similar ICs 1 and 5 from infomax, ICs 3 and 1 from sobi, and ICs 1 and 5 from acsobiro, we would find jade identifies more features than the other methods. In addition, we also observed that infomax is able to extract the spatial activity maps with high contrast though with strong background noise. The main advantages of infomax algorithms based on the minimization of mutual information are its ability to adapt to variations in the environment and the fact that it is robust if the right type of distribution is provided (super- or sub-Gaussian).[20]

Both principal component analysis (PCA) and ICA could be used to extract independent neural sources or reduce the measurements into a smaller set of components. There are significant differences between the two blind source separation methods: (1) PCA uses the first and second moments of the measurements, hence relying heavily on Gaussian features while ICA exploits inherently non-Gaussian features of the data and utilizes higher order moments; (2) PCA maximizes the variance of the projected data along orthogonal direction while ICA finds the vectors onto which the projections are independent; and (3) in PCA, the first principle component accounts for as much of the variability in the data as possible, and each successive orthogonal component accounts for as much of the residual variability as possible while with ICA, we must first choose the number of sources to compute. Both ICA and PCA could be applied to the same problem and the results would be quite different. For example, in "cocktail party effect,"[19,20] ICA is able to distinguish the voice of each independent speaker from the linear combination of the voices while PCA fails to do that.

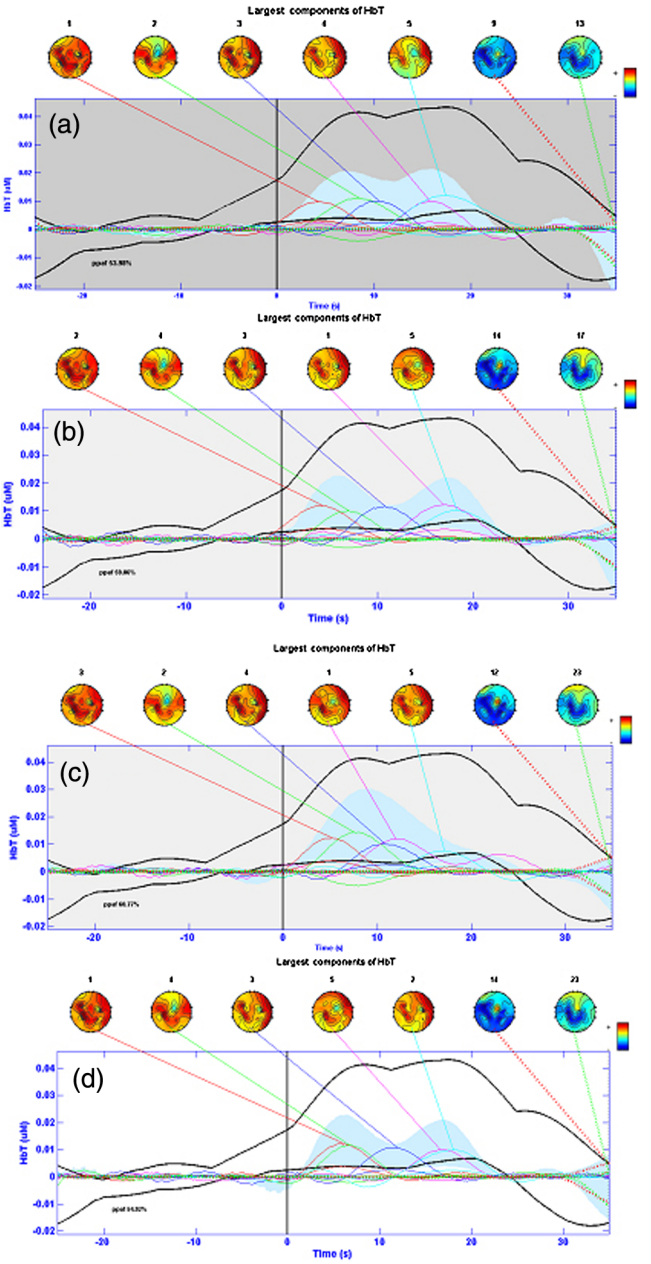

Fig. 7 The spatiotemporal analysis of ICs that contribute the most to the HbT measurements using infomax (a), jade (b), sobi (c), and acsobiro (d) ICA methods. The black thick lines indicate the data envelope (i.e., minimum and maximum of all channels at every time point) and the colored lines show the components of HbT. No significant differences for the calculated ICs among the four methods were observed.

Importantly, recent work[13] on fNIRS shows that ICA has significant advantages on source separations in comparison with PCA.

It is noted that five conditions should be satisfied to perform ICA and PCA: the source signals must be statistically independent; the number of source signals must be equal to the number of mixed observed signals and mixtures must be linearly independent from each other; the model must be noise free; data must be centered; and the source signals must not have Gaussian probability density functions. Further investigations on ICA should include ICA for nonlinear mixing process, ICA for source signals that are noisy, ICA for a number of source

signals greater than the number of observables and blind source separation techniques based on temporal dependencies.[20]

In conclusion, we introduce ICA for fNIRS brain signal processing. The significance of this work is that ICA is able to identify sites of cortical activations and characterize the hemodynamic task responses in time-frequency domain for the whole brain with the event-related components. With further application to more complex tasks, ICA will likely reveal brain dynamics not identified with conventional fNIRS analysis methods.

Acknowledgments

This research was supported by SRG Grant from University of Macau in Macau. In particular, we thank Prof. Jong Chui Ye at KAIST for providing us the fNIRS datasets for our initial methodology study.

References

1. F. F. Jobsis, "Noninvasive, infrared monitoring of cerebral and myocardial oxygen sufficiency and circulatory parameters," *Science* **198**(4323), 1264–1267 (1977).
2. A. Yodh and B. Chance, "Spectroscopy and imaging with diffusing light," *Phys. Today* **48**(3), 34–40 (1995).
3. S. Tak et al., "Quantification of $CMRO_2$ without hypercapnia using simultaneous near-infrared spectroscopy and fMRI measurements," *Phys. Med. Biol.* **55**(11), 3249–3269 (2010).
4. S. G. Diamond et al., "Dynamic physiological modeling for functional diffuse optical tomography," *Neuroimage* **30**(1), 88–101 (2006).
5. Y. Hoshi, "Functional near-infrared optical imaging: utility and limitations in human brain mapping," *Psychophysiology* **40**(4), 511–520, (2003).
6. A. K. Singh et al., "Spatial registration of multichannel multi-subject fNIRS data to MNI space without MRI," *Neuroimage* **27**(4), 842–851 (2005).
7. T. Huppert et al., "Homer: a review of time-series analysis methods for near-infrared spectroscopy of the brain," *Appl. Opt.* **48**(10), 280–298 (2009).
8. P. H. Koh et al., "Functional optical signal analysis: a software tool for near-infrared spectroscopy data processing incorporating statistical parametric mapping," *J. Biomed. Opt.* **12**(6), 064010 (2007).
9. J. C. Ye et al., "NIRS-SPM: statistical parametric mapping for near-infrared spectroscopy," *Neuroimage* **44**(2), 428–447 (2009).
10. C. B. Akgül, A. Akin, and B. Sankur, "Extraction of cognitive activity-related waveforms from functional near-infrared spectroscopy signals," *Med. Biol. Eng. Comput.* **44**(11), 945–958 (2006).
11. T. Katura et al., "Extracting task-related activation components from optical topography measurement using independent components analysis," *J. Biomed. Opt.* **13**(5), 054008 (2008).
12. S. Kohno et al., "Removal of the skin blood flow artifact in functional near-infrared spectroscopic imaging data through independent component analysis," *J. Biomed. Opt.* **12**(6), 062111 (2007).
13. J. Markham et al., "Blind identification of evoked human brain activity with independent component analysis of optical data," *Hum. Brain Mapp.* **30**(8), 2382–2392 (2009).
14. A. V. Medvedev et al., "Event-related fast optical signal in a rapid object recognition task: improving detection by the independent component analysis," *Brain Res.* **1236**, 145–158 (2008).
15. G. Morren et al., "Detection of fast neuronal signals in the motor cortex from functional near infrared spectroscopy measurements using independent component analysis," *Med. Biol. Eng. Comput.* **42**(1), 92–99 (2004).
16. I. Schelkanova and V. Toronov, "Independent component analysis of broadband near-infrared spectroscopy data acquired on adult human head," *Biomed. Opt. Express* **3**(1), 64–74 (2012).
17. H. Zhang et al., "Functional connectivity as revealed by independent component analysis of resting-state fNIRS measurements," *Neuroimage* **51**, 1150–1161 (2010).
18. A. J. Bell and T. J. Sejnowski, "An information-maximization approach to blind separation and blind deconvolution," *Neural Comput.* **7**(6), 1129–1159 (1995).
19. A. Delorme and S. Makeig, "EEGLAB: an open source toolbox for analysis of single-trial EEG dynamics including independent component analysis," *J. Neurosci. Methods* **134**(1), 9–21 (2004).
20. D. Langlois, S. Chartier, and G. Gosselin, "An introduction to independent component analysis: InfoMax and FastICA algorithms," *Tutorials Quant. Methods Psychol.* **6**, 31–38 (2010).
21. http://bisp.kaist.ac.kr/NIRS-SPM.
22. http://sccn.ucsd.edu/wiki/EEGLAB.